The Aeronautical Journal (2023), **127**, pp. 2068–2081
doi:10.1017/aer.2023.94

REGULAR PAPER

Deployable optics for the Buccaneer Main Mission (BMM)

F. Agenbag[1], P.S. Alvino[1], D.C. Bandara[2], H.E. Bennett[1], M. Hollick[1], A.M. James[3], J. Kaduparambil-Jose[2], D.M. Lingard[1], F. Lorenzin[1], B. Lucas[2], A. McKinnon[2], J.D. Nelson[2], C.V. Peck[1], C. Raddock[2], A. Raj[2], P.C.L. Stephenson[4], A. Strachan[2], T. Teske[2] and P. Thornton[2]

[1]Space Autonomy Group, Defence Science & Technology Group, Edinburgh, SA, Australia, [2]Research Engineering, Defence Science & Technology Group, Edinburgh, SA, Australia, [3]University of South Australia, Mawson Lakes Campus, Mawson Lakes, SA, Australia and [4]Resilient Imaging Systems Group, Defence Science & Technology Group, Edinburgh, SA, Australia
Corresponding author: F. Agenbag; Email: Franke.Agenbag1@defence.gov.au

Received: 29 April 2023; **Revised:** 5 September 2023; **Accepted:** 19 September 2023

Keywords: Nanosatellite; CubeSat; Deployable Optics; Imaging System; AIT / AIV; new space

Abstract

Defence Science and Technology Group (DSTG) is currently preparing for the launch of the Buccaneer Main Mission (BMM) satellite, the successor to the Buccaneer Risk Mitigation Mission (BRMM). BMM hosts a high-frequency (HF) antenna and receiver to contribute to the calibration of the Jindalee Operational Radar Network (JORN). Verification of the successful deployment and stability of the large HF antenna is critical to the success of the mission. A bespoke deployable optics payload has been developed by DSTG to fulfil the dual purpose of direct verification of the deployed state of the HF antenna and capturing images of the Earth through a rotatable, dual-surfaced mirror and a variable-focus liquid lens. The payload advances research at DSTG in several fields of space engineering, including deployable mechanisms, precision actuation devices, radiation-tolerant electronics, advanced metal polishing and optical metrology. This paper discusses the payload design, material selection, trade-offs considered for the deployable optics payload and preliminary test results.

Nomenclature

3D	three dimensional
ANSTO	Australian Nuclear Science & Technology Organisation
ANU	Australian National University
BLDC	brushless direct current
BMM	Buccaneer Main Mission
BRMM	Buccaneer Risk Mitigation Mission
CCD	charge coupled device
CMOS	complementary metal oxide semiconductor
CRC	Collaborative Research Centre
CRC	Cyclic Redundancy Check
°C	degrees Celsius
DC	direct current
DSTG	Defence, Science & Technology Group
ECC	Error Correction Code
ECSS	European Cooperation for Space Standardization
EM	engineering model

A version of this paper first appeared at The Australian International Aerospace Congress 2023 (AIAC20).

© Commonwealth of Australia, 2023. Published by Cambridge University Press on behalf of Royal Aeronautical Society. This is an Open Access article, distributed under the terms of the Creative Commons Attribution-NonCommercial-NoDerivatives licence (http://creativecommons.org/licenses/by-nc-nd/4.0/), which permits non-commercial re-use, distribution, and reproduction in any medium, provided that no alterations are made and the original article is properly cited. The written permission of Cambridge University Press must be obtained prior to any commercial use and/or adaptation of the article.

https://doi.org/10.1017/aer.2023.94 Published online by Cambridge University Press

FDIR	fault detection isolation and recovery
FM	flight model
FPGA	field programmable gate array
GATRI	gamma technology research irradiator
GEVS	general environmental verification standards
GigE	gigabit ethernet
GNC	guidance navigation and control
Gy	grey
HF	high frequency
HIAF	heavy ion accelerator facility
I2C	inter-integrated circuit
ISO	International Organisation for Standardisation
JORN	Jindalee Operational Radar Network
kg	kilogram
km	kilometre
LEO	low Earth orbit
m	metre
MANTIS	Manoeuvrable ANtenna Terrestrial and self-Imaging System
MeV	mega electron-volt
mm	millimetre
NAND	Not And
NASA	National Aeronautics and Space Administration
NCRIS	National Collaborative Research Infrastructure Strategy
Pa	pascal
PCB	printed circuit board
PEEK	polyetheretherketone
PV	peak to valley
PWM	pulse width modulation
RMS	root mean square
SECDED	Single Error Correction and Double Error Detection
SEM	Soft Error Mitigation
SPDT	single point diamond turning
SWAP	size, weight and power
TID	total ionising dose
TMR	Triple Modular Redundancy
TVAC	Thermal Vacuum Chamber
UART	Universal Asynchronous Receiver-Transmitter
UHF	Ultra High Frequency
UV	ultraviolet
WRESAT	Weapons Research Establishment Satellite

1.0 Introduction

The Buccaneer CubeSat programme is the first sovereignly developed defence satellite programme flown by Australia since the Weapons Research Establishment Satellite (WRESAT) in 1967. The Australian project consists of two missions: Buccaneer Risk Mitigation Mission (BRMM) and Buccaneer Main Mission (BMM). The programme entails two key objectives; (1) exploring calibration of the Jindalee Operational Radar Network (JORN) from space using a high-frequency (HF) receiver payload; and (2) to train a cadre of Australian Defence satellite engineers and operators. BRMM was a 3U CubeSat developed in partnership with the University of New South Wales Canberra. BRMM was successfully launched into a sun-synchronous low Earth orbit (LEO) by the National Aeronautics and Space Administration (NASA) in November 2017, from the Vandenberg Air Force Base in California. The lessons learned from BRMM served as a risk reduction activity for BMM [8]. BMM is a 6U CubeSat

https://doi.org/10.1017/aer.2023.94 Published online by Cambridge University Press

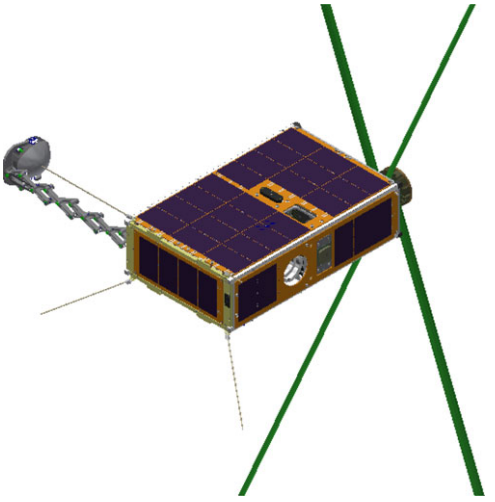

Figure 1. *Buccaneer Main Mission CubeSat with UHF antenna (gold), part of HF antenna (green) and MANTIS payload (grey) deployed.*

(Fig. 1) and will be launched into a sun-synchronous orbit, approximately 500km altitude, in mid-2024. BMM will utilise an improved primary payload design, based on the heritage gained from the risk mitigation mission, to allow JORN radar signals that have been partially refracted by the ionosphere to be collected in LEO.

In addition to the primary HF payload, BMM houses a secondary payload for further space to ground experimentation and novel scientific investigation. This payload includes an optical communications system for space to ground communications, an iridium transceiver for satellite to satellite communications and a deployable optics instrument known as the Manoeuvrable Antenna Terrestrial and self-Imaging System (MANTIS).The inclusion of an optical communications payload is motivated by a need for high data rates and broadening the available electromagnetic spectrum to be used, with an Optical Ground Station currently under development at DSTG [11].

MANTIS contains a self-imaging and Earth-imaging electro-optic sensor with a catadioptric imaging system. The mirror components are stowed during launch and deployed on-orbit with a scissor-mechanism boom. The three objectives of this payload are to:

1. Confirm the successful deployment of external components, including the primary payload's HF antenna, by acquiring images of the entire satellite with the wide-field configuration of the imaging system.
2. Monitor any degradation of the camera system over time through imagery of a robust reference chart on the exterior surface of the satellite. Image quality (sharpness and colour rendition) will be monitored. Of particular interest is the on-orbit performance of the liquid-lens component of the sensor which has no space heritage.
3. Demonstrate the ability to manipulate the deployed mirrors at the end of the boom arm to capture images of the Earth with a narrow-field configuration of the imaging system.

In collaboration with the Australian Centre for Field Robotics at the University of Sydney, and the SmartSat CRC, whose activities are funded by the Australian government's Cooperative Research Centres (CRC) program, a planned secondary objective using MANTIS is to demonstrate goal-oriented algorithms and software on orbit that will grant a spacecraft mission-autonomy capability to undertake

https://doi.org/10.1017/aer.2023.94 Published online by Cambridge University Press

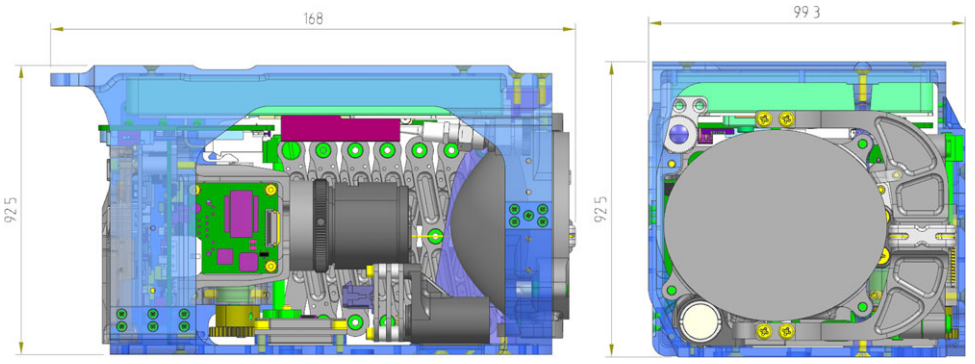

Figure 2. *MANTIS payload stowed inside housing (side view).*

self-inspection autonomously and adaptively in real-time. These goal-driven on-board autonomy activities intend to demonstrate novel scientific innovation in accordance with the latest CubeSat trends for future applications [17]. This could serve applications including fault detection isolation and recovery (FDIR) and guidance navigation and control (GNC).

The significance of BMM is that it marks an important milestone in small satellite innovation for Australian Defence, experiments with new capabilities to maintain the performance of an important Defence asset in JORN, and introduces new capabilities to the Australian space ecosystem such as space-to-space communications via Iridium, and optical communications. Finally, a number of novel space engineering innovations are demonstrated through the MANTIS payload and will be tested in the space environment; including the first known use of a liquid-lens in space to focus objects at different distances, and a novel mechanism for extending and retracting mirrors to deploy a large catadioptric optical system.

2.0 Conceptual design

Satellites commonly house imaging systems for Earth observation and climate observation; however, observing their immediate surroundings and exterior self-inspection is rare [2], and space manipulator systems even rarer [14]. Imaging systems with adjustable focus allow the surroundings of the satellite to be imaged at variable distances. Traditionally, these systems require complex and reliable mechanical movement, the difficulties of which are amplified in the space environment due to exposure to high shock and vibration loads, thermal extremes, vacuum-induced cold welding and high-energy radiation. The use of a liquid lens for adjustable focusing removes one complex mechanical system from the optical chain.

For CubeSats, deployable structures overcome the increased size, weight, and power (SWAP) constraints imposed by the need to fit into standard CubeSat dispenser pods. Various groups have worked on deployable optical structures for CubeSats: these range from deployable membranes that act as photon sieve diffractive optics [3], to rigid deployable mirrors [16], and wire-driven systems [1]. However, these systems are primarily focused on maximising ground sampling distance within the significant SWAP constraint for CubeSat systems, in contrast to our objectives of an adjustable focus instrument for self-inspection and Earth observation; and manipulation and retractability.

Other key features of the MANTIS payload are its deployable and retractable arm, and its rotatable, dual-surfaced mirror (Figs. 2–5). The former allows the imaging system to remain within the envelope of the satellite for launch and when the payload is not in use (Fig. 2), advancing research towards precision actuation of space optics. The latter facilitates dual-purpose imaging, with the convex-surfaced mirror providing images of the satellite, including the entirety of the 3.4m-long HF antenna, and the flat surfaced

https://doi.org/10.1017/aer.2023.94 Published online by Cambridge University Press

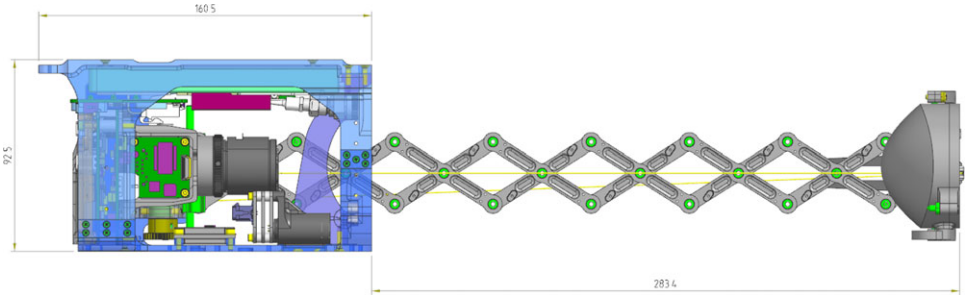

Figure 3. *MANTIS payload fully deployed with convex-surfaced mirror facing the satellite for self-imaging (top view).*

Figure 4. *MANTIS payload fully deployed with convex-surfaced mirror facing satellite for self-imaging (side view).*

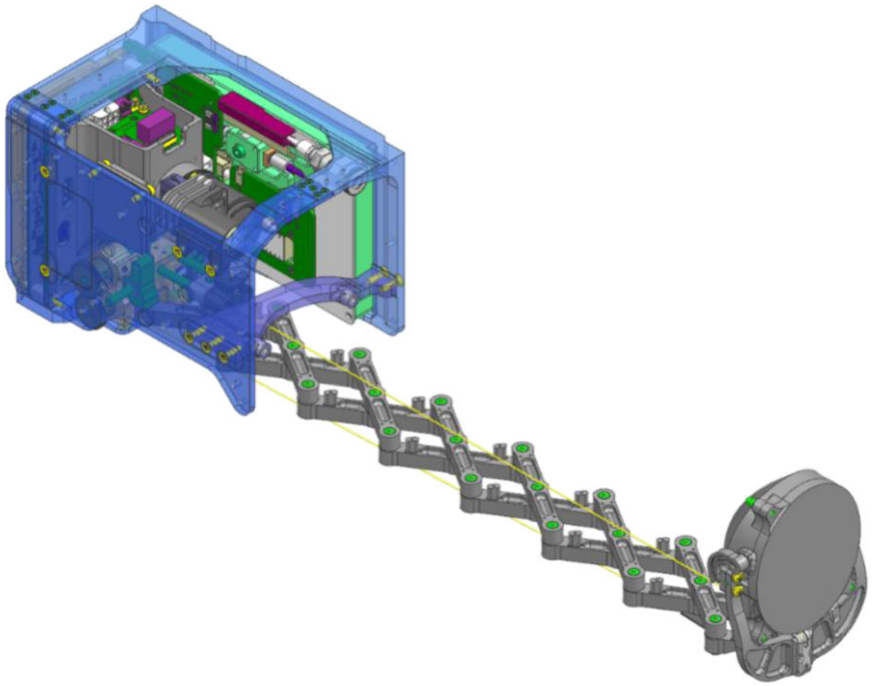

Figure 5. *MANTIS payload fully deployed with convex-surfaced mirror facing satellite for self-imaging (isometric view).*

https://doi.org/10.1017/aer.2023.94 Published online by Cambridge University Press

mirror capturing images of the Earth. The use of a deployable, rotatable mirror was the outcome of a trade study conducted during the conceptual design phase of the payload where field-of-view, volumetric efficiency and aperture minimisation were the main criteria.

The MANTIS payload includes several key elements being tested for flight heritage. The electro-optic imaging sensor features a FLIR Blackfly S GigE CMOS camera, and a Corning Varioptic variable focus liquid lens as part of the imaging optics. A complementary metal oxide semiconductor (CMOS) sensor was selected above its charge coupled device (CCD) counterpart due to the sensor requiring less voltage and current to operate. The liquid lens allows the focal length to be changed between the two imaging modes. Fine adjustments to mitigate temperature-dependent focus shifts of the remaining optical elements will also be possible. Focus changes are achieved electronically, without moving parts, making it more robust to the thermal extremes and hard vacuum of the space environment than traditional lens systems.

3.0 Rotatable mirror

The selection of a payload architecture involving a deployed rotatable mirror necessitated mirror actuation at a distance from the satellite and the payload electronics. In order to achieve this, an internal geared motor assembly was designed, with actuation roughly about its centre of gravity to reduce torque requirements. The design could also accommodate a redundant motor if required if failure occurs due to vibration on launch, thermal load impact or radiation exposure. With this drive arrangement, the mirror can rotate through 135 degrees, which is sufficient to achieve the dual imaging objectives. Precision control of the mirror's rotation is achieved through eccentric bushings that allow the gear spacing inside the mirror to be adjusted to remove backlash between meshing gears, and an incremental encoder coupled to the gear shaft to measure the actual mirror rotation. As an incremental encoder rather than an absolute encoder is used for registering angular position, the need for a repeatable reference position is required. The reference position is designed such that the mirror is always first reversed to the reference position before any commands are given. Once the reference position has been identified via engagement of a limit switch, all further movements of the mirror are calibrated back to the starting reference position. Minimisation of the backlash between the gear teeth was a challenge that was overcome with the use of elliptical adjustment which enabled backlash to be minimised. The reduction of backlash was important in order to ensure that the mirror position output coincides with the desired set point. The mirror is manufactured from aluminium-6061 T651, primarily due to its low density and low melting point, resulting in low atmospheric re-entry risk. Titanium was initially considered for the mirror due to its relative ease of polishing and ability to be 3D printed at DSTG; however, its high melting point and thus high chance of surviving atmospheric re-entry rendered its use infeasible [15]. The aluminium mirror was conventionally manufactured in two pieces, both with a thickness of 2mm to provide adequate radiation shielding for a 12-month mission lifetime in LEO, and to allow surfacing using single-point diamond machine-turning (SPDT).

The two deployed mirror surfaces have an elliptical outline with principal dimensions 60 and 70mm. The flat mirror surface after SPDT has a surface roughness of not greater than 15nm root mean square (RMS), and a form error approximately 2.3 fringes peak to valley (PV). The convex mirror surface is a hyperbolic conic section of revolution, designed to give a total field of view of greater than 200 degrees when used in combination with the 35mm focal length lens and the FLIR detector. Surface roughness of not greater than 9.2nm RMS was achieved through the SPDT surfacing. This level of surface roughness is sufficiently low to achieve only modest levels of light scatter, suitable for the present mission [7]. Various coatings were considered to reduce the possibility of reflectivity reduction in aluminium primarily in the ultraviolet (UV) spectrum caused by exposure to atomic oxygen [4, 19]. However, given the short mission duration and risk of introducing thermal expansion effects, no further surface polishing nor coatings were applied to either surface given the expected resilience of the grade of mirror substrate used.

https://doi.org/10.1017/aer.2023.94 Published online by Cambridge University Press

A Maxon three-phase brushless DC (BLDC) motor with a 1:1024 gearhead ratio was selected to control mirror rotation due to its space heritage and testing to ISO9100 standards [10]. Braycote grease was installed in the motor by Maxon to ensure low-outgassing vacuum compatibility. The motor is fitted with a 512-step optical encoder to measure mirror rotation. The encoder selection took into account effects of shock and vibration during launch and how this may introduce air gaps between the detector and disk encoder components. Limit switches in the payload electronics register when the mirror is at the upper or lower limit of rotation (0 degrees and 135 degrees, respectively) and trigger a software interrupt to prevent the motor driving the mirror beyond its intended limits.

Motor positional control is achieved using an STSPIN32F0 BLDC controller with an embedded STM32 microcontroller, which is located on a printed circuit board (PCB) embedded within the mirror. The motor is driven using six-step commutation based on feedback from the motor's integrated hall effect sensors; operating as open-loop system at start-up and then switching to a closed-loop control system once feedback from the hall effect sensors becomes more reliable at higher speeds. This is implemented in firmware using three complementary pulse width modulation (PWM) timers which in turn are controlled by a single timer interrupt for hall effect sensor feedback. A finite state machine is used to handle commands from the satellite bus, as well as any motor faults such as stall conditions or start-up failure.

4.0 Retractable arm

The requirements for retractability and precision deployment drove the design trade-offs for the mirror deployment mechanism. Passive deployment mechanisms, such as bistable carbon-fibre booms in novel cross-sections, which are commonly used in satellite deployable systems, were excluded during the conceptual design phase of the project due to their failure to meet the retractability, and deployment stability and repeatability requirements. Mechanically driven telescopic booms, such as the deployable membrane telescope payload from the US Air Force academy [3], were the next design class to be eliminated due to their very high manufacturing tolerance requirements combined with the high risk of cold welding between sliding surfaces. The most volumetrically efficient and reliable retractable deployment mechanism identified in the conceptual design phase was a 'scissor' mechanism.

The scissor mechanism is made of several pieces of aluminium 6061-T651, with the material selected for the same reasons as the mirror, detailed above. The risk of cold welding between the sliding members of similar metal is mitigated by using polyetheretherketone (PEEK) bushings in the arm joints. Each joint in the arm houses a custom-designed torsion spring, which is compressed during scissor mechanism retraction and when in the stowed configuration, providing stored potential energy that is used during deployment. A motor-driven 0.6mm 7×7 G316 stainless steel wire cable wraps around the scissor arm to control its rate and degree of extension, and to collapse the scissor mechanism during retraction. The cable drum is grooved to ensure the cable is spooled precisely without overlap during extension and retraction. The torsion spring-cable system provides a highly volume-efficient extension-retraction mechanism and removes backlash from each arm segment. At full extension, the mechanism measures 230mm.

The mirror and scissor arm assembly is compressed onto three tapered pins via the cable in its stowed launch configuration to restrict all modes of translation and rotation during launch vibration. The mirror is guided off the tapered pins during deployment, and a thin titanium guide is used to maintain the mirror orientation at 90 degrees to the axis of the camera. The mirror mechanism is isolated from the scissor mechanism and satellite via lower stiffness isolators, which acts to attenuate any on-board vibration that may be transmitted to the mirror.

Deployment and retraction of the scissor arm is achieved using the same Maxon BLDC motors and gearboxes as the mirror, with the encoder attached to the cable drum to record drum rotations and therefore the deployment distance of the mirror relative to the camera. A second BLDC controller located within the payload body provides positional control of the motor using a similar control algorithm to that used for the mirror. Limit switches are again used to trigger software interrupts which prevent the arm

https://doi.org/10.1017/aer.2023.94 Published online by Cambridge University Press

from over-extending which could cause the scissor-mechanism cable to snap, or over-retracting which could cause the mirror to collide with the camera.

The entire secondary payload including MANTIS is housed in an aluminium 6061-T6 chassis which is manufactured in two sections for ease of manufacturability and assembly. The MANTIS chassis then integrates as one piece into the BMM satellite chassis to mitigate the risk of mechanical interface incompatibilities. The field-programmable gate array (FPGA) that controls the MANTIS camera, and the MANTIS camera itself, both require heatsinks to dissipate heat generated during their operation. These aluminium blocks are bonded to their respective components through thermal pads, and connected to cold parts of the MANTIS chassis via thermally conductive heat straps.

5.0 Imaging system

The imaging system integrated into the MANTIS payload is the first known example of liquid lens technology to be prepared for launch on a satellite, with NASA's Fluidic Telescope experiment (FLUTE) the only other known work [9]. Liquid lenses were not specifically designed with space applications in mind; however, they present considerable potential for use within the space environment.

The catadioptric imaging system comprises a mirror and a commercial camera lens that incorporates a liquid lens element. The mirror component is one of a pair of deployable mirrors on an approximately 30cm extendable scissor-action beam. The mirrors can be exchanged by rotating either the planar mirror or the convex mirror into the optical train using an electric motor within the mirror shell. The convex surface is a conic one whose curvature converts the approximately 10° field of view of the lens and detector plane to 220° field of view to image the satellite and its deployed HF antennae.

The camera lens is an Edmund Optics Cx series 35mm focal length f/5 C-mount lens (catalogue number #33-676) that includes a Corning Varioptic A-39N0 liquid lens element for focus adjustment. This lens element is a cell containing two immiscible liquids between parallel planar glass windows with a clear circular aperture diameter of 3.9mm. The curvature of the interface surface between the two liquids creates the optical power of the lens, and is controlled by the application of a voltage across the cell that changes the interface-to-wall contact angle via the electrowetting principle [12]. The near-identical density of the two liquids ensures that surface tension forces dominate any gravitational or inertial forces on the interface surface shape. Changing the applied voltage changes the optical power of the lens element within the range −15.0D to +25.6D. Power changes are rapid, repeatable and cover the range required of the system to focus either in the far distance through the planar mirror for Earth observation, or near distance through the convex mirror for a wide field-of-view image of the host satellite. Minor focus adjustments are limited only by the precision of the applied voltage; in the present case, to 0.01V or approximately 0.008D optical power change. These adjustments can be used to accommodate system changes due, for example, to temperature variations or launch displacement.

The liquid lens focussing element provides a wide range of focus with fine adjustment, within a very small volume; is relatively inexpensive to incorporate into the sensor design; and is robust, having no mechanical moving parts. With no prior space heritage, it was unknown how such a lens would perform on orbit, and whether it would degrade in the space environment. Consequently, during the design phase, sample liquid lens elements were subjected to a range of tests to determine the suitability of their use in orbit. These tests included: thermal cycling, vacuum out-gassing, vibration, displacement damage and total ionising dose radiation. The test lenses were examined for changes in structural and optical performance and were found to be unchanged under test conditions (described below) appropriate for a LEO satellite.

The MANTIS payload involved the development of software to drive the imaging system and the deployable arm/mirror, including the implementation of a variety of space environment software mitigation techniques to achieve a high-reliability design for use in space-based applications. Achieving high reliability was relevant to both software and hardware components. Software reliability required a variety of considerations including error avoidance, error detection, error removal and fault-tolerance.

https://doi.org/10.1017/aer.2023.94 Published online by Cambridge University Press

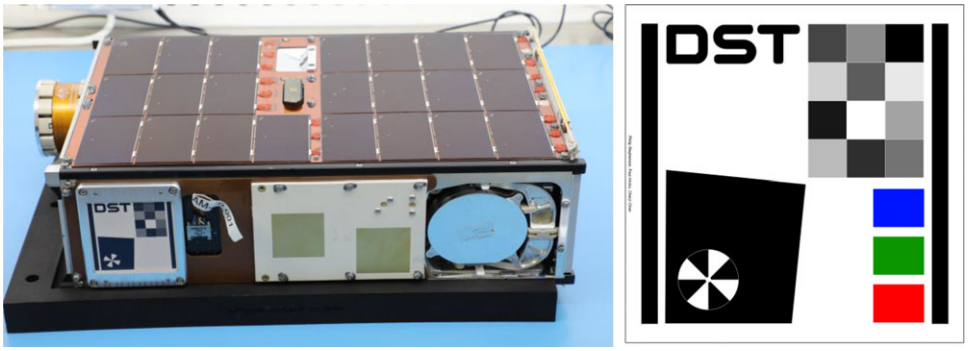

Figure 6. *(left) The MANTIS payload and resolution chart integrated into the Buccaneer Main Mission (BMM) Engineering Model (EM); the resolution chart can be observed on the left side of the spacecraft, and the external facing flat mirror of MANTIS on the right. (right) Image of the updated resolution chart to be integrated into the Flight Model (FM) spacecraft.*

Hardware reliability focused on the system's tolerance to environmental effects. An FPGA was utilised to control the camera unit, with the FPGA featuring high computational density, efficiency across applications and re-programmability through reconfiguration. FPGAs have extensive flight history, particularly in LEO [10].

Controlling the liquid lens involved several considerations, including appropriate ranges of applied voltage (with the goal of minimising optical aberrations), effective optical distances and suitable focal adjustments. Earth-based systems that implement variable focus on liquid lens technology were drawn upon for code development. The imaging system was configured in a development environment using a Xilinx KCU-705 development board, prior to being implemented on the FPGA. To apply voltage to the lens, a driver board was utilised. The driver board communicated with the microcontroller through I2C protocol, and the developed lens code allowed for the transmission of hexadecimal values, which correlated to voltage values within the focal range. Commands for manual focus were implemented, such as focusing the system at infinity, which will be used on orbit for imaging Earth.

To assist monitoring any sensor imaging degradation while on orbit, a resolution chart is attached to the side of the of the satellite being imaged by MANTIS. The chart is a white-ceramic substrate on which has been printed a set of greyscale patches and slanted-edge patterns in blue chrome. There are also three patches of printed epoxy colour ink (red, green, and blue). The slanted-edge patch will be used to assess image quality through the measurement of the sensor line-spread function, and it includes a star pattern to assist in image focusing. The greyscale and colour patches are to be used to assess sensor response and colour rendition. An image of a prototype chart (without colour patches) attached to the BMM EM is shown on the left-hand side of the satellite in Fig. 6. The optimal location adjacent to the MANTIS payload on the right-hand side could not be achieved due to the location of the S-band communication antenna.

6.0 Fault tolerant design

Achieving high reliability was an important consideration when designing the payload hardware, as well as the FPGA firmware and all embedded software. Hardware reliability focused on the system's tolerance to environmental effects, achieved through the use of radiation tolerant components and shielding. The decision was made not to use a radiation-hardened FPGA due to cost, but rather to pair an industry-grade FPGA with a radiation-hardened Not-And (NAND) flash memory bank to store the FPGA bit stream and bootloader.

https://doi.org/10.1017/aer.2023.94 Published online by Cambridge University Press

Triple modular redundancy (TMR) was initially considered to provide fault tolerance within the FPGA firmware, but this was eventually discarded due to a lack of resources within the FPGA. Instead, a configuration scrubber was implemented based on a hybrid scrubber architecture as proposed by Stoddard et al. [18]. This approach utilises the speed of the FPGA's internal read-back hardware, while maintaining the robustness of an external configuration scrubber.

To achieve this, the Xilinx Soft Error Mitigation (SEM) IP core was utilised to perform single error correction and double error detection (SECDED) and an MSP430 microcontroller was used to monitor a UART output from the SEM controller. When the SEM controller detects an error which it is unable to repair on its own, such as multiple bit-flips occurring within a single memory frame, it alerts the microcontroller, which then retrieves an uncorrupted copy of the bit stream from the radiation-hardened memory and uses this to reprogram the affected memory frame.

An additional benefit of this approach is that multiple bit streams can be stored within the memory concurrently, and the microcontroller can then switch between multiple bit streams and load new firmware into the FPGA with minimal delay. New bit streams can also be uploaded over the air to implement software and firmware changes while in orbit, while maintaining the original bit stream in case the system needs to fall back to a safe state.

To provide a final layer of resilience at a software level, cyclic redundancy checks (CRCs) and error correction codes (ECCs) were appended to all critical data stored in the on board memory, and CRCs were also built into all payload commands.

Based on this design and radiation modelling performed, the ECSS radiation design margin [5] was determined to be approximately 10 for the MANTIS internal mirror electronics and liquid lenses, thus requiring radiation lot testing; and greater than 10 for all remaining components of the MANTIS payload, thus not requiring radiation lot testing. These tests are described below.

7.0 Environmental testing and reliability

The ability of the mirror and arm assembly to function as intended after exposure to launch and thermal loads, and radiation degradation, has been verified at the payload assembly and sub-assembly level. At a component level, various high-risk spacecraft components were radiation tested to ensure their reliability over a one-year mission life. At an assembly level, a custom vacuum-compatible test rig was designed to enable repeatable testing of the scissor mechanism, and it has been successfully extended and retracted over 100 times in the laboratory to provide the design team with confidence in its reliability. The payload will be tested again at a fully integrated satellite level during the environmental test campaign of the satellite. The results of the sub-assembly and assembly test campaign are summarised below and indicate that the system is suitable for extended operations in LEO.

The liquid lenses and mirror electronics were radiation tested at component level to indicate the possible damage on orbit during the expected mission lifetime of approximately one year. To investigate total ionising dose (TID) damage, the gamma technology research irradiator (GATRI) at the Australian Nuclear Science & Technology Organisation (ANSTO) was used to produce the representative TID using a cobalt-60 radioisotope. The test samples were contained within two polyethylene plates, unshielded and placed within the GATRI test chamber where the cobalt-60 rods were raised out of their safety chamber, resulting in exposure of the sample to gamma rays with a distribution of energies between 1.17 and 1.33MeV [6]. These gamma ray energies result in Compton scattering dominating the interaction effect, simulating the ionisation experienced in orbit. The mirror electronics were continuously monitored during the test. It was not possible to continuously monitor the optical performances of the test lenses during radiation exposure, so different test lens samples were exposed to four progressively increasing doses of radiation (at the equivalent of 3, 6, 9 and 12 months of exposure – 50, 100, 150 and 200Gy) and the optical performance subsequently tested. No optical performance degradation was observed in any lenses; however, the RS-485 transceiver inside the mirror electronics was damaged in all samples after an equivalent radiation exposure of approximately 12 months. To mitigate this failure, the aluminium mirror thickness was increased to 2mm, increasing the predicted mission life from one year to five years.

https://doi.org/10.1017/aer.2023.94 Published online by Cambridge University Press

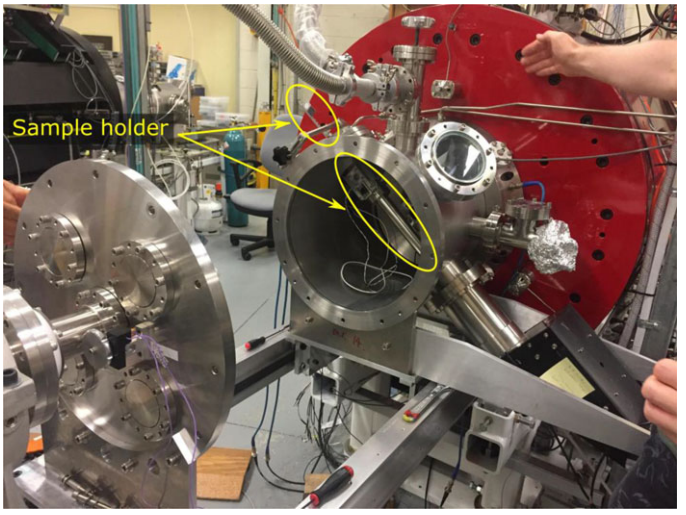

Figure 7. *Test setup of the lens being loaded into the Heavy Ion Accelerator Facility at the Australian National University. The lens can be seen in the sample holder (indicated) ready for loading inside the cylindrical vacuum chamber.*

Additionally, the lens susceptibility to displacement damage was measured by exposing the lens to sufficiently high proton energies required to produce atomic displacements; thus a fixed proton energy of 25 MeV was selected. For this test, the Heavy Ion Accelerator Facility (HIAF) at the Australian National University (ANU) was used to produce the proton beams, the only facility in Australia capable of providing high-energy proton beams. At this single proton energy, the satellite experiences a fluence of 1.28×10^7/cm^2/MeV over its 12-month mission life. However due to an early calculation error, the full-period mission dose applied was slightly higher at 1.8×10^7/cm^2/MeV. As in the TID test, it was not possible to continuously monitor the optical performances of the test lenses during radiation exposure, so different test lens samples were exposed to four progressively increasing doses of radiation (at the equivalent of 3, 6, 9 and 12 months of exposure). The test setup is shown in Fig. 7. No optical performance degradation was observed in any lenses.

To the authors knowledge, this is the first Australian space radiation testing performed on an Australian space payload.

To simulate launch loads, the assembled MANTIS payload was subjected to random and sine vibration levels defined in the NASA General Environmental Verification Standard (GEVS) [13] for spacecraft below 22.7kg. The random vibration profile was performed at "qualification levels" (the recommended limit level + 3dB) and the slopes between frequency values was maintained at ±6dB/oct, with the duration of each random vibration totalling 2 minutes per axis. GEVs test levels envelope the levels of vibration anticipated by most current launch vehicles, and these test levels were applied to each axis of the MANTIS assembly. A single axis test is shown in Fig. 8. The pre-to-post random vibration change in first mode peaks was negligible in all axes and both orientations, indicating no major physical changes to the payload, which was confirmed during physical inspection and functional testing at the end of the vibration campaign.

To simulate the extreme temperature cycling experienced in orbit, NASA General Environmental Verification Specification (GEVS) [13] requires four thermal cycles between temperatures that exceed the expected on-orbit component temperature range by at least 10C, at a pressure less than 1×10^{-5} Torr (1.33×10^{-3}Pa), for qualification of subsystems, instruments and payloads. The number of cycles for qualification at component level increases to eight. The assembled MANTIS payload underwent eight thermal vacuum cycles from −30°C to 60°C with a test-chamber pressure less than 1×10^{-5} Torr (1.33×10^{-3}Pa). The test setup is shown in Fig. 9. The temperature change rate was 1°C/min between

https://doi.org/10.1017/aer.2023.94 Published online by Cambridge University Press

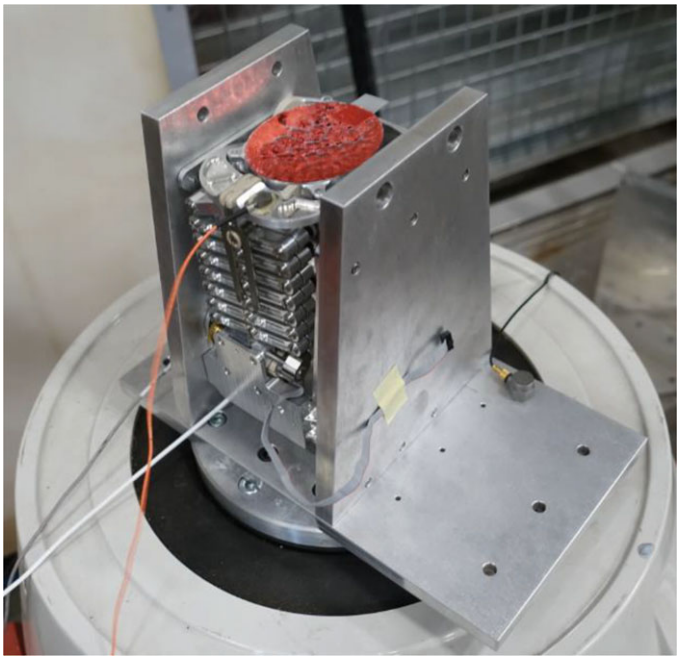

Figure 8. *Test setup of the MANTIS assembly being fixed onto the Bruel and Kjaer LDS V721 Shaker table at DSTG.*

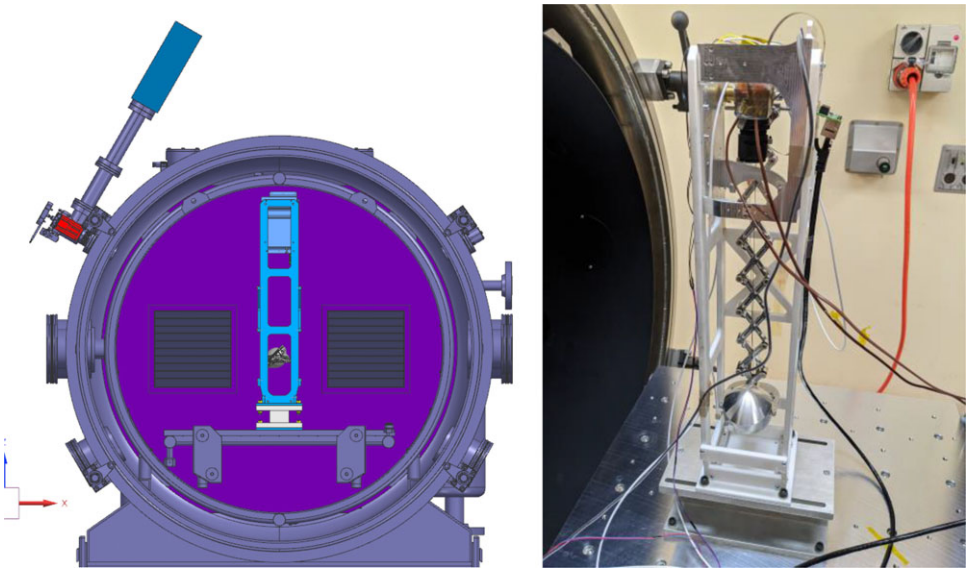

Figure 9. *Test setup of the MANTIS payload Thermal Vacuum Chamber (TVAC) testing at DSTG. (left) Bi-section of the TVAC with the MANTIS thermoplastic deployment jig. (right) Initial setup of the MANTIS arm being fully extended on the TVAC platen; this extension was performed during each thermal cycle dwell period.*

https://doi.org/10.1017/aer.2023.94 Published online by Cambridge University Press

these limits, and the payload was held at the temperature extremes for a dwell time of 1 hour. A ninth thermal cycle was also performed where the MANTIS payload was dwelled for 5 minutes at each 10°C interval from −30°C to 60°C. During each dwell time, the MANTIS arm was fully extended, 15 images were captured, and the arm was fully retracted. No faults in the payload were observed under temperature and pressure extremes.

8.0 Conclusion

This project advances Australian space-based deployable optics in several ways, including space qualification of a self-inspection payload, liquid lens and extending/retracting deployment mechanism; polishing techniques for optical surfaces; and advancement of capabilities required for segmented deployable optics in space that will facilitate the formation of large apertures on small spacecraft.

Acknowledgement. The author/s acknowledge the facilities, and the scientific and technical assistance provided by Heavy Ion Accelerators (HIA). HIA is supported by the Australian Government through the National Collaborative Research Infrastructure Strategy (NCRIS) program.

References

[1] Aglietti, G.S., Honeth, M., Gensemer, S. and Diegel, O. Deployable optics for CubeSats, 2020, https://digitalcommons.usu.edu/cgi/viewcontent.cgi?article=4737&context=smalls

[2] Asphericon. Satellite Cameras, 2020, https://www.asphericon.com/en/applications/aerospace-industry/satellite-cameras#:~:text=Functionality%20of%20satellites%20for%20earth,events%20on%20earth%20in%20detail.&text=Camera%20systems%20in%20satellites%20can,from%20ultraviolet%20to%20infrared%20beams

[3] Dearborn, M.E., Anderson, G.P., Asmolova, O., Balthazor, R.L., McHarg, M.G., Nelson, H.C., Quiller, T.S., Wilson, G.R., Harvey, T.J. and Murphey, T.W. A deployable membrane telescope payload for cubesats, *J. Small Satellites*, 2014, pp 253–264, https://jossonline.com/wp-content/uploads/2021/08/0301-Dearborn-A-Deployable-Membrane-Telescope.pdf

[4] Dooling, D. Material selection guidelines to limit atomic oxygen effects on spacecraft surfaces. Marshall Space Flight Centre, 1999, https://s3vi.ndc.nasa.gov/ssri-kb/static/resources/19990064119.pdf

[5] ECSS, E. ECSS-Q-ST-60-15C Radiation Hardness Assurance-EEE Components. ECSS Secretariat, 2012, https://ecss.nl/standard/ecss-q-st-60-15c-radiation-hardness-assurance-eee-components-1-october-2012/

[6] European Space Agency. Total Dose Steady State Irradiation Test Method, European Space Components Coordination (ESCC) Basic Specification No. 22900, Issue 5, European Space Agency, 2016, http://escies.org/escc-specs/published/22900.pdf

[7] Hashima, H. and Burrows, C.J. Effect of mirror microroughness scattering on the Hubble Space Telescope point spread function, in *Space Astronomical Telescopes and Instruments II*, 1993, https://www.spiedigitallibrary.org/conference-proceedings-of-spie/1945/1/Effect-of-mirror-microroughness-scattering-on-the-Hubble-Space-Telescope/10.1117/12.158788.full?SSO=1

[8] Hollick, M., Lingard, D., Stevens, N., Peck, C., Alvino, P., Duong, H., Hu, G. and Van Antwerpen, C. Buccaneer risk mitigation mission operations – lessons learnt, 69th International Astronautical Congress (IAC), Bremen, Germany, 1-5 October, 2018, doi: IAC-18-B4,3,7,x42484

[9] Luria, O., Elgarisi, M., Frumkin, V., Razin, A., Ericson, J., Gommed, K., Widerker, D., Gabay, I., Belikov, R., Bookbinder, J., Balaban, E. and Bercovici, M. Fluidic Shaping and in-situ Measurement of Liquid Lenses in Microgravity, 2022, arXiv preprint arXiv:2212.08139.

[10] Maxon Group. ISO 9100 DC motors for the Aerospace industry, 2023, www.maxongroup.net.au/maxon/view/content/aerospace

[11] Mudge, K., Clare, B., Jager, E., Devrelis, V., Bennet, F., Copeland, M., Herrald, N., Price, I., Lechner, G., Kodithuwakkuge, J., Magarelli, J., Bandara, D., Peck, C., Hollick, M., Alvino, P., Camp-Smith, P., Szumylo, B., Raj, A. and Grant, K. DSTG laser satellite communications -current activities and future outlook, IEEE International Conference on Space Optical Systems and Applications (ICSOS), Kyoto City, Japan, 2022, pp 17–21, doi: 10.1109/ICSOS53063.2022.9749716

[12] Mugele, F. and Baret, J.C. Electrowetting: from basics to applications, *J. Phys. Condens. Matter,* 2005, **17**, pp 705–774, https://iopscience.iop.org/article/10.1088/0953-8984/17/28/R01

[13] NASA. General Environmental Verification Standard (GEVS) for GSFC Flight Programs and Projects, NASA Goddard Space Flight Center (GSFC), Greenbelt, 2021, https://standards.nasa.gov/standard/GSFC/GSFC-STD-7000

[14] Papadopoulos, E., Aghili, F., Ma, O. and Lampariello, R. Robotic manipulation and capture in space: A survey, *Front. Rob. AI*, 2021, **228**, https://www.frontiersin.org/articles/10.3389/frobt.2021.686723/full

[15] Roulet, M., Atkins, C., Hugot, E., Lemared, S., Lombardo, S. and Ferrari, M. 3D printing for astronomical mirrors, in *3D Printed Optics and Additive Photonic Manufacturing*, Vol. **10675**, 2018, p 1067504, https://arxiv.org/pdf/2011.01000

[16] Schwartz, N., Pearson, D., Todd, S., Milanova, M., Brzozowski, W., Vick, A., Lunney, D., MacLeod, D., Greenland, S., Sauvage, J.F. and Gore, B. Laboratory demonstration of an active optics system for high-resolution deployable CubeSat, 2018, arXiv:1809.09097.

[17] Segret, B. and Mosser, B. Autonomous Orbit Determination for a CubeSat Cruising in Deep Space, 2021, arXiv:2104.09989[astro-ph.IM].

[18] Stoddard, A., Gruwell, A., Zabriskie, P. and Wirthlin M.J. A hybrid approach to FPGA configuration scrubbing, *IEEE Trans. Nuclear Sci.*, 2016, p 99, https://www.researchgate.net/publication/311498600_A_Hybrid_Approach_to_FPGA_Configuration_Scrubbing

[19] Ter Horst, R., Tromp, N., de Haan, M., Navarro, R., Venema, L. and Pragt, J. Directly polished lightweight aluminium mirror, in *Advanced Optical and Mechanical Technologies in Telescopes and Instrumentation,* Vol. **7018**, 2008, pp 63–72, https://www.spiedigitallibrary.org/conference-proceedings-ofspie/10566/105660P/Directly-polished-lightweight-mirror/10.1117/12.2308200.full

Cite this article: Agenbag F., Alvino P.S., Bandara D.C., Bennett H.E., Hollick M., James A.M., Kaduparambil-Jose J., Lingard D.M., Lorenzin F., Lucas B., McKinnon A., Nelson J.D., Peck C.V., Raddock C., Raj A., Stephenson P.C.L., Strachan A., Teske T. and Thornton P. (2023). Deployable optics for the Buccaneer Main Mission (BMM). *The Aeronautical Journal*, **127**, 2068–2081. https://doi.org/10.1017/aer.2023.94

https://doi.org/10.1017/aer.2023.94 Published online by Cambridge University Press